Chinese Chemical Letters 35 (2024) 109165

Contents lists available at ScienceDirect

Chinese Chemical Letters

journal homepage: www.elsevier.com/locate/cclet

A nitroreductase-responsive nanoprobe with homogeneous composition and high loading for preoperative non-invasive tumor imaging and intraoperative guidance

Jingqi Xin[a,b], Shupeng Han[b], Meichen Zheng[b], Chenfeng Xu[c], Zhongxi Huang[c], Bin Wang[d], Changmin Yu[c], Feifei An[b,*], Yu Ren[d,*]

[a] Institute of Medical Engineering, Department of Biophysics, School of Basic Medical Science, Health Science Center, Xi'an Jiaotong University, Xi'an 710061, China
[b] School of Public Health, Health Science Center, Xi'an Jiaotong University, Xi'an 710061, China
[c] Key Laboratory of Flexible Electronics (KLOFE) & Institute of Advanced Materials (IAM), Nanjing Tech University, Nanjing 211816, China
[d] Department of Breast Surgery, the First Affiliated Hospital of Xi'an Jiaotong University, Xi'an 710061, China

ARTICLE INFO

Article history:
Received 13 August 2023
Revised 24 September 2023
Accepted 3 October 2023
Available online 5 October 2023

Keywords:
Nitroreductase
Tumor diagnosis
Intraoperative guidance
Self-assembly
Nanoprobe

ABSTRACT

Tumor microenvironment (TME)-activatable probes have been proven to effectively increase signal-to-background ratios (SBRs) and improve the success rate of complete tumor resection. However, many fluorescence probes have to be loaded into a nanocarrier for tumor targeted delivery, which consequently encounters poor drug loading, heterogeneous composition and non-encapsulated drug aggregates occurred during nanoformulation fabrications. Herein, a nitroreductase (NTR)-activated "OFF-ON" near-infrared fluorescence nanoprobe, named NanoBodipy, was synthesized by the spontaneous self-assembling of NTR-responsive dye-polyethylene glycol (PEG) amphiphilic polymer in water. The NTR-responsive dye acted as the hydrophobic segment in the amphiphilic polymer, yielding a homogeneous composition and a high loading of 12.2 wt% (according to calculation) in the synthesized NanoBodipy. The synthesized NanoBodipy can efficiently accumulate in tumors *via* the enhanced permeability and retention (EPR) effect, enabling non-invasive tumor-targeted fluorescence imaging and guiding complete tumor resection. Once the synthesized NanoBodipy entered the tumor cells, they dissociated and were activated by overexpressed NTR. With the real-time fluorescence guide of NanoBodipy, complete tumor resection surgery was performed successfully.

Tumor fluorescence imaging enables non-invasive and precise diagnosis of tumors, even those with small sizes [1,2]. Compared to pathologic analysis of tissues, tumor fluorescence imaging offers a better way to intraoperatively determine tumor margins with less time consumption and improved precision [3–5]. As a result, tumor fluorescence imaging has become an important technology for tumor diagnosis and is applied in clinic [6,7]. With the assistance of tumor-targeted fluorescence nanoprobes, fluorescence imaging-guided tumor resection surgery can be performed with reduced surgical hazards and increased probabilities of complete tumor resection [8–10]. However, conventional fluorescence probes often suffer from poor signal-to-background ratios (SBRs) [11–13], which triggered the demand of designing tumor microenvironment (TME) activatable probes.

It is well-known that TME activatable fluorescence probes can switch their fluorescence from an "OFF" state to an "ON" state in response to TME indicators, which not only amplifies the signal at the tumor site but also minimizes the background signal in normal tissues [14–16]. Consequently, the SBRs can be increased, resulting in improved bioimaging contrast [17–19]. It is widely recognized that nitroreductase (NTR) is overexpressed in many tumors and has been explored as a TME factor to design smart probes with increased SBRs for tumor detection [20–24]. Hence, an NTR-activated "OFF-ON" fluorescence probe possessing increased SBRs can be a powerful tool for non-invasive tumor diagnosis [25,26]. However, most smart fluorescence probes intrinsically lack the ability of tumor-targeted accumulation and need to be integrated into various drug delivery platforms, especially nanocarriers [27].

* Corresponding authors.
E-mail addresses: anfeifei@xjtu.edu.cn (F. An), renyyyyy@xjtufh.edu.cn (Y. Ren).

https://doi.org/10.1016/j.cclet.2023.109165
1001-8417/

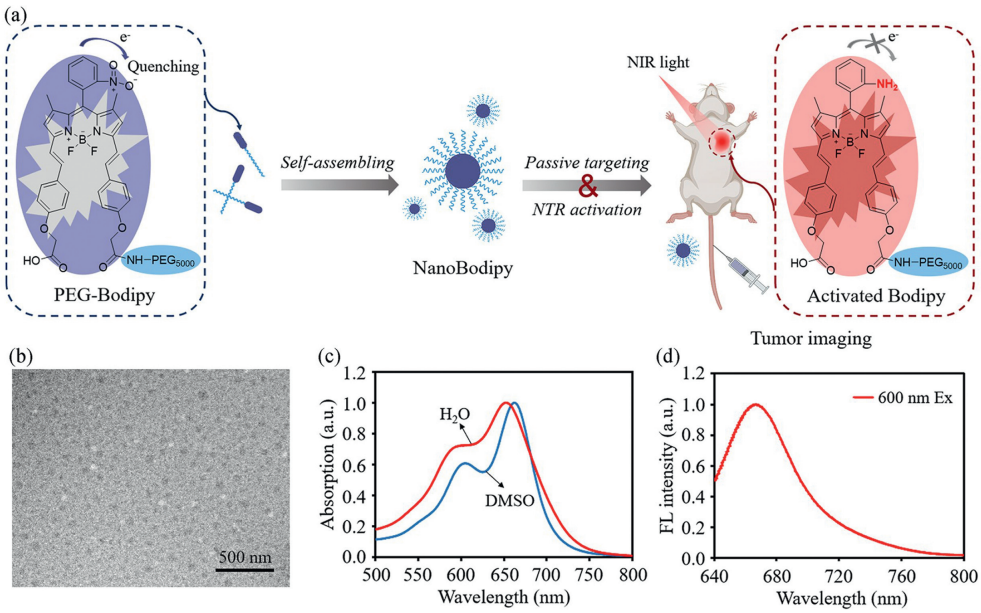

Fig. 1. (a) Schematic response mechanism of tumor-targeted NIR fluorescence imaging achieved by self-assembled NTR-activated nanoprobe NanoBodipy. (b–d) Characterization of NanoBodipy. (b) TEM image of NanoBodipy. Scale bar: 500 nm. (c) UV-visible-NIR absorbance spectrum of NanoBodipy in deionized water and dimethyl sulfoxide (DMSO). (d) Fluorescence spectrum of activated NanoBodipy in Tris buffer containing 3% DMSO.

Nevertheless, the poor drug loading resulted in a large volume of drug solution for further intravenous injection, heterogeneous nanomedicine composition and non-encapsulated drug aggregates occurred during nanoformulation fabrications, which have posed challenges for optimizing the nanoprobe systems [28,29]. In order to overcome these drawbacks, various strategies for designing nanocarriers have been explored in recent years [30–33].

Herein, an NTR-activatable "OFF-ON" near-infrared (NIR) fluorescence nanoprobe, called NanoBodipy, was synthesized by conjugating a hydrophobic bodipy dye with a hydrophilic polyethylene glycol (PEG) chain, which further self-assembled into a nanoprobe spontaneously (Fig. S1 in Supporting information). The synthesized NanoBodipy possessed a fixed composition and a significantly high loading (12.2 wt% according to calculation). In addition, the synthesized NanoBodipy itself plays a role in assisting drug delivery with less use of inert materials, thus achieving a high drug loading capacity and low toxicity. *In vitro* tests demonstrated that the synthesized NanoBodipy can be selectively activated by NTR in solution and switch on its fluorescence in cancer cells under TME-mimic hypoxic conditions. Further *in vivo* studies demonstrated that NanoBodipy can achieve tumor-targeted fluorescence imaging by the dual-effects of passive targeting and NTR activation. After intravenous injection, NanoBodipy accumulated at the tumor by enhanced permeability and retention (EPR) effect. When NanoBodipy entered tumor cells, they dissociated into amphiphilic PEG-Bodipy molecules in the intracellular lipophilic environment and was further activated into fluorescent Bodipy by the overexpressed NTR, accompanying with the disappearance of electron-withdrawing effect (Fig. 1a) [34–36]. Importantly, NanoBodipy can accurately determine the tumor margins and provide intraoperative guidance for complete tumor resection by real-time fluorescence imaging. The hematoxylin and eosin (H&E) staining images of major organs slices and blood biochemical analysis confirmed the biocompatibility of the synthesized NanoBodipy.

Aiming for targeted imaging of *in vivo* hypoxic tumor, an efficient NTR-activated fluorescent probe NanoBodipy was designed. NanoBodipy fabricated based on bodipy has an NIR optical window and displayed enhanced fluorescence for increased light penetrability and minimal interference from autofluorescence [37–39]. The synthesis of PEG-Bodipy involved three steps, as shown in Fig. S1. Firstly, 2-nitrobenzene was introduced into the bodipy scaffold as a switch for NTR activation, obtaining G-Bodipy. Secondly, the 3,5-positions of the bodipy were substituted with 4-formylphenoxyacetic acid to obtain R-Bodipy. With an extended π conjugation system, the maximum excitation and emission peaks of R-Bodipy were tuned into the NIR region, enhancing the light penetrability, and reducing autofluorescence interference. Lastly, R-Bodipy was conjugated with a PEG chain to obtain PEG-Bodipy for enhanced biocompatibility. As shown in Fig. S2 (Supporting information), the synthetic R-Bodipy was identified to be pure. The high-resolution MS (HRMS) spectrum suggested that the formula of R-Bodipy was $C_{37}H_{30}BF_2N_3O_8$ with a mass of 692.2149, which were in accordance with the structure and chemical molecular weight of R-Bodipy (Fig. S3 in Supporting information). The HPLC profile in Fig. S4 (Supporting information) demonstrated the purity of the synthesized R-Bodipy, with a retention time of 14.146 min. As shown in Fig. S5 (Supporting information), ^{1}H nuclear magnetic resonance (NMR) spectrum of PEG-Bodipy exhibited the characteristic peaks of both Bodipy and PEG chains, confirming that R-Bodipy was successfully conjugated with PEG chains. According to Fig. S6 in Supporting information, the matrix-assisted laser desorption/ionization time-of-flight mass spectrometry (MALDI-TOF MS) spectrum of PEG-Bodipy exhibited a molecular weight of approximately 5700, which was consistent with the predicted chemical molecular weight of PEG-Bodipy. In addition, there is no signal observed at the molecular weight of approximately 10,000 in the MALDI-TOF MS, suggesting that PEG modification only happen to one -COOH in the R-Bodipy, ascribed to the steric hindrance. The above results provided confirmation of the successful synthesis of R-Bodipy and PEG-Bodipy. An effective NTR-catalyzed reaction was preformed depending on enzyme-probe binding, enzyme catalysis and finally product departure processes. The binding capability between probe and NTR is vital for the following catalysis and departure steps. Thus, docking experiments were performed to evaluate the binding preference of PEG-Bodipy towards NTR, then preliminarily investigate the practicability of the design of the NTR-activated probe. However, owing to the unduly large molecular weight of PEG-Bodipy, the calculation was failed to perform. Thus,

R-Bodipy was substituted for PEG-Bodipy to investigate the binding capability between probe and NTR. As shown in Fig. S7a (Supporting information), the distance between R-Bodipy and NTR were determined to be between 1.8–2.2 Å, the short distance favored the efficient probe-enzyme interaction. The probe-binding sites was delineated to be ASN-41, LYS-75, SER-76, LYS-173 and GLN-98 (Figs. S7b–d in Supporting information). In addition, the binding energy value of enzyme-probe complexes was estimated to be −6.89 kcal/mol, suggesting the interaction between R-Bodipy and NTR (Table S1 in Supporting information). Flavin mononucleotide (FMN) group as the active site of NTR plays an important role in the redox reaction. The distance between R-Bodipy and FMN-300 was determined to be 10 Å (≤10 Å), suggesting that R-Bodipy enabled to interact with NTR. However, the -COOH of R-Bodipy was considered to have a great influence of binding capability. As shown in Fig. S8a (Supporting information), a new molecule (like-PEG-Bodipy) was designed to simulate the PEG-Bodipy. Then, the binding capability of the new molecule and NTR was investigated (Figs. S8a–d in Supporting information). The distance between like-PEG-Bodipy and NTR was determined to be between 2.0–2.2 Å. The binding sites were determined to be GLN-98, SER-76 and LYS-75. Furthermore, the binding energy value of enzyme-substitute complexes was estimated to be −7.28 kcal/mol (Table S2 in Supporting information). The distance between like-PEG-Bodipy and FMN-300 was determined to be 8.0 Å (≤10 Å), suggesting that like-PEG-Bodipy enabled to interact with NTR. The quantitative docking results of R-Bodipy and like-PEG-Bodipy provided the first line of evidence that NanoBodipy might be an "OFF-ON" probe activated by NTR.

Preparation and characterization of NanoBodipy are shown as below. The amphiphilicity of PEG-Bodipy enabled the self-assembly of NanoBodipy during the dialysis. As shown in Fig. S9 (Supporting information), critical micelle concentration value of NanoBodipy was 1.375 μmol/L, which was defined by pyrene 1:3 ratio method, indicating the self-assembly of NanoBodipy. The size of NanoBodipy (≈100 nm) detected by the transmission electron microscopy (TEM) and dynamic light scattering (DLS) showed that NanoBodipy can accumulate in tumor *via* an enhanced EPR effect (Fig. 1b and Fig. S10 in Supporting information). Plus, TEM result showed that NanoBodipy exhibited a spherical morphology with a relatively uniform size. The results revealed that conjugating hydrophobic compound with a PEG chain is a simple but effective method to fabricate self-assembled nanomicelles with excellent performance. Furthermore, the size stability results showed that NanoBodipy was stable in 24 h in water and 1× phosphate buffered saline (PBS, pH 7.4), but slightly coagulative in 48 h (Fig. S11 in Supporting information). However, NanoBodipy could accumulate into tumor *via* EPR effect even with the coagulation for its slight size enlargements.

For the further application, the absorbance and emission of NanoBodipy were investigated. The UV–visible-NIR absorption spectrum of NanoBodipy displayed a maximum absorption peak at a wavelength of 652 nm in water and 662 nm in DMSO (Fig. 1c). To observe the emission of activated NanoBodipy, the probe was incubated with NTR in Tris buffer, and characterized with a fluorescence spectrum. The fluorescence spectrum exhibited that the emission of activated NanoBodipy maximized at 666 nm (Fig. 1d). The spectra revealed that both absorption and emission of NanoBodipy were red-shifted to the NIR region (650–900 nm) resulting from the extension of π conjugation system [40,41].

To assess the extent of the NTR reaction, the fluorescence intensity response of NanoBodipy was recorded at various time points (0–140 min). Fig. 2a showed that the fluorescence intensity was continuously increased up to ∼2.3-fold at 120 min upon the addition of 10 μg/mL NTR, suggesting that NanoBodipy could be effectively activated by NTR. Furthermore, to evaluate the selectivity of NanoBodipy for NTR, various potential interfering species were examined, including metal ions (Ca^{2+}, K^{+}, Mg^{2+}, Na^{+}, Cu^{2+}), common carbohydrate (glucose, sucrose, polysaccharide), amino acids (L-glutamate, L-arginine, glycine), reducing agent carbamide and oxidizing agent H_2O_2. Interfering species had little influence on the NanoBodipy activation, compared to activation triggered by NTR (Fig. 2b). The results indicated that NanoBodipy possessed sensitivity and specificity for NTR activation.

The fluorescence images of NanoBodipy in 4T1 breast cancer cells and L929 normal cells were further obtained to investigate whether NanoBodipy was specifically and intensively activated in 4T1 cancer cells under hypoxic conditions. The images (Fig. 2c) showed strong fluorescence in 4T1 cells cultured under hypoxic conditions but little fluorescence in 4T1 cells cultured under normoxic conditions. In addition, fluorescence was hardly observed in L929 cells cultured under both hypoxic and normoxic conditions, indicating that NanoBodipy could be effectively and specifically activated in 4T1 cancer cells with NTR overexpression under hypoxic conditions. To further confirm the specific activation of NanoBodipy, the relative fluorescence intensities of 4T1 cells and L929 cells cultured under different conditions were measured after 24 h of incubation (Fig. 2d). The results suggested that 4T1 cells cultured under hypoxic conditions exhibited ∼30-fold stronger fluorescence compared to 4T1 cells cultured under normoxic conditions, confirming the efficient activation of the probe by the overexpressed NTR. Moreover, 4T1 cells cultured under hypoxic conditions exhibited more than 30-fold stronger fluorescence compared to L929 cells cultured under both hypoxic and normoxic conditions, confirming the specific activation of NanoBodipy in cancer cells which overexpressed NTR under hypoxic conditions. Notably, a higher fluorescence increase of NanoBodipy was observed in the cell fluorescence imaging compared to that measured in the PBS buffer. This phenomenon can be ascribed to steric hindrance and aggregation-induced fluorescence quenching. In the PBS buffer, the amphiphilic PEG-Bodipy self-assembled into nanomicelles (NanoBodipy), which made it difficult for the probe to be recognized and activated by NTR due to the steric hindrance. In addition, even if amphiphilic PEG-Bodipy was activated by NTR and regained its strong fluorescence, it can still maintain the status of a nanomicelle and exhibited aggregation-induced fluorescence quenching. In comparison, when NanoBodipy was endocytosed into the cancer cells, it will dissociate into amphiphilic PEG-Bodipy molecules and be activated by the overexpressed NTR in the lipophilic intracellular environment. Therefore, the cell fluorescence imaging exhibited a much stronger fluorescence response than that in the PBS buffer.

In addition, cell cytoviabilities of 4T1 breast cancer cells and human umbilical vein endothelial cells (HUVEC) normal cells were carried out to evaluate the biological safety of NanoBodipy. The results suggested that NanoBodipy was nontoxic to the cells (Fig. S12 in Supporting information). As shown in Fig. S13 (Supporting information), the red blood cells (RBCs) remain intact and precipitates at the bottom in all the NanoBodipy solutions, contrarily, hemolysis occurs in control group. The results showed that the fraction of hemolysis in all concentrations of NanoBodipy are less than 0.5%, demonstrating that the NanoBodipy did not cause hemolysis of RBCs even at a concentration as high as 500 μg/mL.

NanoBodipy, designed as the specific tumor-targeting fluorescent probe, was further monitored fluorescence emission in xenograft tumor mouse models *in vivo* and *ex vivo*. The animal study was approved by the Biomedical Ethics Committee of Xi'an Jiaotong University Health Science Center (No. 2021–1612). The 4T1 tumor-bearing mice were intravenously injected with NanoBodipy (200 μL, 0.486 mg/mL), then imaged at 2, 8 and 24 h. As depicted in Fig. 3a, obvious fluorescence signals in tumors revealed that NanoBodipy rapidly accumulated at the tumor tissue and activated by tumor-overexpressed NTR, even at 2 h post injection.

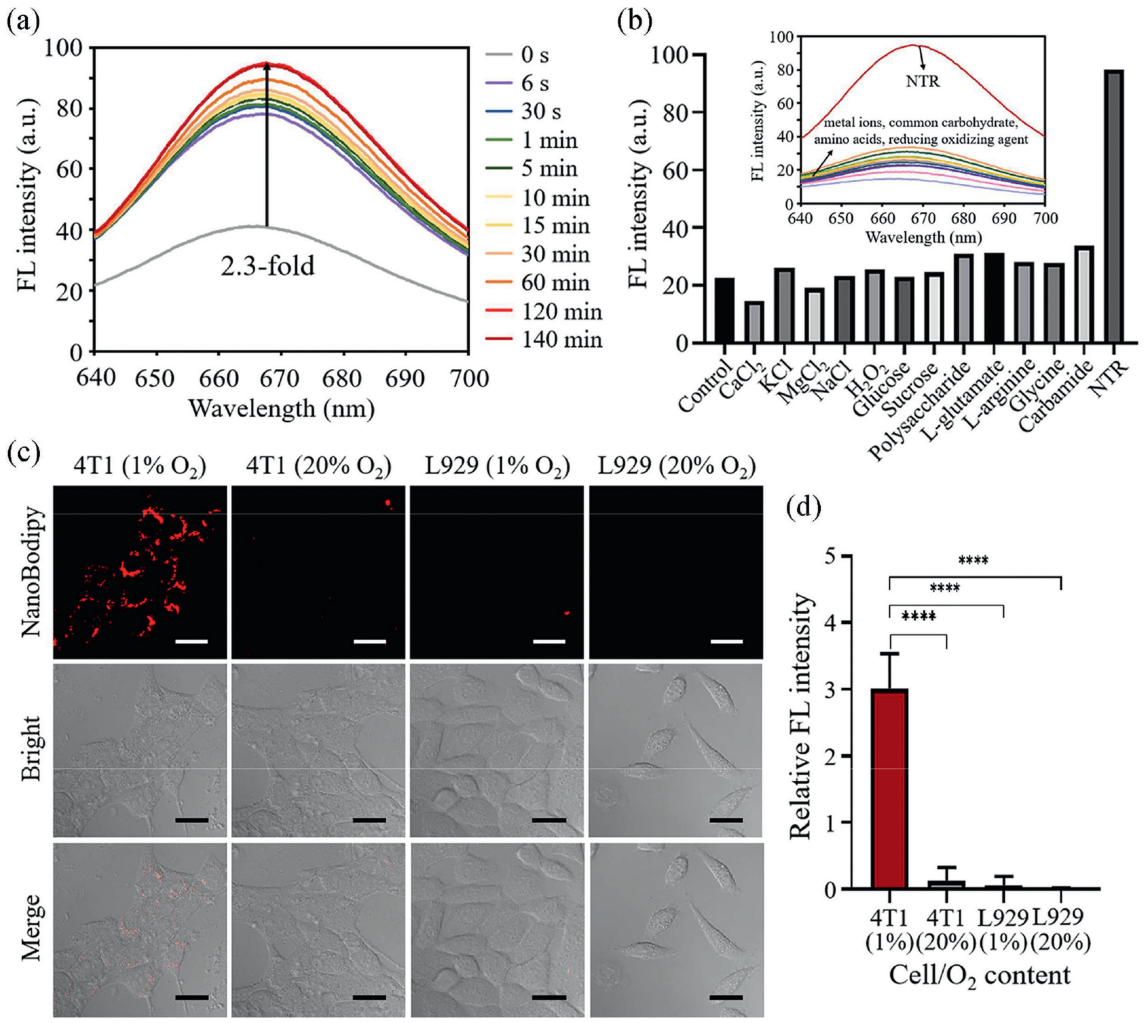

Fig. 2. Sensitivity and selectivity of NanoBodipy for NTR activation in the solution and in the cells. (a) Fluorescence emission spectrum of NanoBodipy reacted with NTR. (b) Fluorescence responses of NanoBodipy (0.5 μmol/L) reacted with various species: control (NanoBodipy + 500 μmol/L NADH) and with $CaCl_2$ (50 mmol/L), KCl (50 mmol/L), $MgCl_2$ (50 mmol/L), NaCl (50 mmol/L), H_2O_2 (1 mmol/L), glucose (10 mmol/L), sucrose (10 mmol/L), polysaccharide (10 mmol/L), L-glutamate (1 mmol/L), L-arginine (1 mmol/L), glycine (1 mmol/L), carbamide (10 mmol/L), and NTR (10 μg/mL). (c) Fluorescence images of 4T1 and L929 cells incubated with NanoBodipy for 24 h. Scale bar: 25 μm. (d) Relative fluorescence intensities of 4T1 and L929 cells incubated with NanoBodipy for 24 h. Each point with an error bar represents the mean ± standard deviation (SD) ($n = 4$). $^{****}P < 0.0001$ (*t*-test).

Furthermore, the NanoBodipy started to exhibit the strongest fluorescent signal in the tumor compared to biotic tissues at 8 h post injection, and this obvious contrast maintained until 24 h post injection, demonstrating the favorable capability of NanoBodipy as a tumor-targeted NTR-activated fluorescent probe. To investigate the metabolism and distribution of NanoBodipy, *ex vivo* fluorescence images of major organs and the tumor were carried out at 8 and 24 h post injection. As shown in Fig. 3b, the tumor maintained strong fluorescence signals until 24 h post-injection, confirming that NanoBodipy can remain in the tumor for an extended period, thus benefiting tumor diagnosis through fluorescence imaging. Additionally, the liver and kidney also exhibited relatively strong fluorescence signals. Previous studies have found that the liver and kidney also have high NTR expression compared to other main organs [42,43], leading to the activation of NanoBodipy probe and strong fluorescence signals in the liver and kidney. The quantitative results revealed that NanoBodipy can persist in tumor for more than 24 h, while being rapidly metabolized in normal tissues, except for the liver and kidney (Fig. 3c). The retained fluorescence signals in the liver and kidney at 24 h post-injection remind us to monitor the possible toxicity of the NanoBodipy probe to the liver and kidney. The above results demonstrated that our probe could be utilized as a prominent bioimaging tool for *in vivo* real-time tumor-targeted imaging.

To further confirm the tumor-targeted capability of NanoBodipy, a fluorescence imaging-guided surgery was performed. As shown in Fig. 4a, the mouse with 4T1 tumor in its right hind leg was imaged firstly to identify the exact location of the tumor before the operation. Then, the tumor was exposed and exhibited more intense fluorescence after cutting into the fur. According to the fluorescence distribution pattern, the tumor was resected and was believed to have been completely removed. However, the strong fluorescence in the surgical incision suggested the residual of the tumor tissue. Guiding by the fluorescence imaging, a second resection was performed to completely remove the tumor issue away from the surrounding musculature. The complete tumor resection was performed with the smallest possible incision, thereby reduced the possibility of incision infection.

To further validate the complete removal of the 4T1 tumor, *ex vivo* fluorescence images and histology examination were conducted on the resected tumor. As shown in Figs. 4b–d, the tumor area exhibited strong red fluorescence, while the normal tissue showed much weaker fluorescence, confirming the accumulation of NanoBodipy at the tumor. The clear tumor margin also

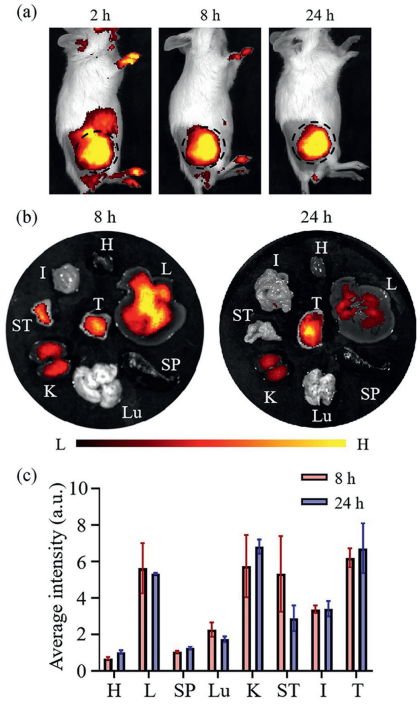

Fig. 3. *In vivo* and *ex vivo* fluorescence images of NanoBodipy at different time points. (a) *In vivo* fluorescence images of 4T1 tumor-bearing mice injected with NanoBodipy at 2, 8 and 24 h. (b) *Ex vivo* fluorescence images of main organs and tumor obtained at 8 and 24 h post-injection. (c) Quantified fluorescence biodistribution of NanoBodipy (H: heart; L: liver; SP: spleen; Lu: lung; K: kidney; ST: stomach; I: intestine; T: tumor). Each point with an error bar represents the mean ± SD ($n = 3$).

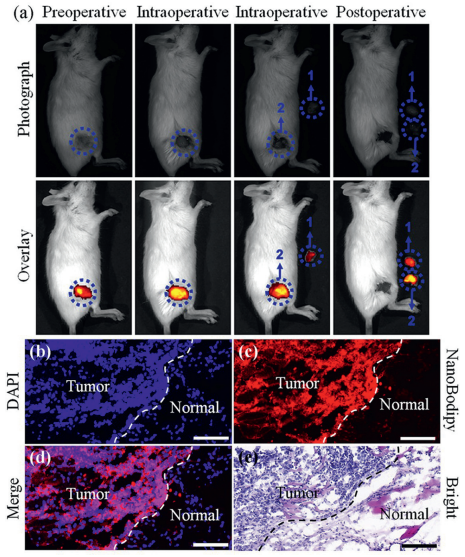

Fig. 4. Intraoperative guidance of NanoBodipy for complete tumor resection by fluorescence imaging. (a) Fluorescence-guided surgery of 4T1 tumor resection. Animal had undergone the surgery at 24 h after injection of NanoBodipy. 1: first resection; 2: second resection. (b–d) *Ex vivo* fluorescence images of 4T1 tumor resected at 24 h post intravenous injection of NanoBodipy. (e) Histology examination of 4T1 tumor resected at 24 h post intravenous injection of NanoBodipy. Scale bar: 100 μm. DAPI: 4′,6-diamidino-2-phenylindole.

confirmed the complete removal of the tumor during the imaging-guided surgery. In addition, the examination of H&E staining of the tumor slice provided additional verification that the tumor was entirely removed from the mouse with the assistance of NanoBodipy guidance (Fig. 4e).

To further verify the biocompatibility of NanoBodipy, the histological investigation of major organs harvested from the mouse at 24 h post-injection was carried out. The results showed that there was negligible organ damage in the sections of the normal organs, indicating that NanoBodipy had good biocompatibility (Fig. S14 in Supporting information). The biochemical tests of NanoBodipy measured at 24 h post injection were carried out. In the biochemical tests, levels of aspartate aminotransferase (AST) and alanine aminotransferase (ALT) were measured as indicators of liver injury, creatinine (CREA) and blood urea nitrogen (BUN) for kidney injury. As shown in Fig. S15 (Supporting information), no significant changes were observed in levels of AST, ALT, CREA and BUN compared with that in the control groups, suggesting that NanoBodipy did not cause any acute toxicity. The mice injected with NanoBodipy solution (17.4 mg/kg) were weighed and their survival ratios were recorded for seven consecutive days, all mice were survival and alive, and gained additional weight slowly in the seven days (Fig. S16 in Supporting information). To further observe their health conditions, blood biochemical tests were carried out, and the results indicated that the liver and renal functions of the mice injected with NanoBodipy solution remained healthy (Fig. S17 in Supporting information). Furthermore, the biocompatibility investigation of NanoBodipy measured and analyzed on the 14th day post injection suggested that NanoBodipy do have good biocompatibility. As shown in Fig. S18 (Supporting information), all the mice were survival, and maintained a healthy body weight in fourteen days. The results of biochemical tests suggested that levels of AST, ALT, CREA and BUN in the mice were in the normal values (Fig. S19 in Supporting information). The above results suggested that the prepared NanoBodipy is highly biocompatible for intravenous injection.

In summary, this article reports on the development of an NTR-activated probe (NanoBodipy) with an NIR optical window based on bodipy dye for tumor-targeted fluorescence imaging. The probe exhibited the expected emission in the NIR region and a fluorescence OFF-ON response *via* the NTR-catalyzed reduction, enabling the smart imaging of hypoxic tumor. With amphiphilicity, PEG-Bodipy molecule can self-assemble into nanomicelles (NanoBodipy) in aqueous solution. The NTR-responsive dye acted as the hydrophobic segment in the amphiphilic polymer, yielding a homogeneous composition and a high loading of 12.2 wt% (according to calculation) in the synthesized NanoBodipy. After accumulation at the tumor *via* EPR effect, the synthesized NanoBodipy was endocytosed by the tumor cells and dissociated into PEG-Bodipy molecules. The dissociated PEG-Bodipy molecules were subsequently activated by NTR overexpressed in tumor and performed tumor-targeted fluorescence imaging. With the assistance of NanoBodipy, complete tumor removal can be achieved under the guidance of fluorescence imaging. Furthermore, NanoBodipy was demonstrated to have excellent *in vivo* biocompatibility according to histological investigation and biochemical tests, highlighting its potential as a clinical optical probe.

Declaration of competing interest

The authors declare that they have no known competing financial interests or personal relationships that could have appeared to influence the work reported in this paper.

Acknowledgments

This study was supported by the National Natural Science Foundation of China (Nos. 51903201, 82172798), the Natural Science Foundation of Shaanxi Province (No. 2023-YBSF-270), the Open Program of NHC Key Laboratory of Nuclear Medicine and Jiangsu

Key Laboratory of Molecular Nuclear Medicine (No. KF202203) and Horizontal Project of the First Affiliated Hospital of Xi'an Jiaotong University (No. 202304174). The characterization assistance from the Instrument Analysis Center of Xi'an Jiaotong University is also acknowledged.

Supplementary materials

Supplementary material associated with this article can be found, in the online version, at doi:10.1016/j.cclet.2023.109165.

References

[1] Z. Zeng, J. Ouyang, L. Sun, et al., Anal. Chem. 92 (2020) 9257–9264.
[2] S. Zheng, W. Huang, N. Li, et al., Chin. Chem. Lett. 34 (2023) 107764.
[3] Z. Hu, C. Fang, B. Li, et al., Nat. Biomed. Eng. 4 (2020) 259–271.
[4] S. Hernot, L. van Manen, P. Debie, J.S.D. Mieog, A.L. Vahrmeijer, Lancet Oncol. 20 (2019) e354–e367.
[5] R. Ito, M. Kamiya, Y. Urano, Curr. Opin. Chem. Biol. 67 (2022) 102112.
[6] H. Li, D. Kim, Q. Yao, et al., Angew. Chem. Int. Ed. 60 (2021) 17268–17289.
[7] J. Xing, Q.Y. Gong, R.F. Zou, et al., Chin. Chem. Lett. 34 (2023) 107786.
[8] A.D. Newton, J.D. Predina, M.H. Shin, et al., Ann. Surg. 270 (2019) 12–20.
[9] W. He, Z. Zhang, Y. Luo, et al., Biomaterials 288 (2022) 121709.
[10] L.J. Lauwerends, P.B.A.A. van Driel, R.J. Baatenburg de Jong, et al., Lancet Oncol. 22 (2021) e186–e195.
[11] P. Wang, Y. Fan, L. Lu, et al., Nat. Commun. 9 (2018) 2898.
[12] B. Li, L. Lu, M. Zhao, Z. Lei, F. Zhang, Angew. Chem. Int. Ed. 57 (2018) 7483–7487.
[13] Q. Yang, Z. Hu, S. Zhu, et al., J. Am. Chem. Soc. 140 (2018) 1715–1724.
[14] H. Chen, Z. Qin, J. Zhao, et al., Biomaterials 225 (2019) 119520.
[15] J. Zhang, P. Cheng, K. Pu, Bioconjug. Chem. 30 (2019) 2089–2101.
[16] W. Chyan, R.T. Raines, ACS Chem. Biol. 13 (2018) 1810–1823.
[17] X.B. Zhao, J.Y. Kang, Y.P. Shi, Anal. Chem. 94 (2022) 6574–6581.
[18] Y. Tian, Y. Li, W.X. Wang, et al., Anal. Chem. 92 (2020) 4244–4250.
[19] Y. Tian, Y. Li, W.L. Jiang, et al., Anal. Chem. 91 (2019) 10901–10907.
[20] F. Xu, H. Li, Q. Yao, et al., Chem. Sci. 10 (2019) 10586–10594.
[21] R. Wang, J. Chen, J. Gao, et al., Chem. Sci. 10 (2019) 7222–7227.
[22] J. Sun, Z. Hu, R. Wang, S. Zhang, X. Zhang, Anal. Chem. 91 (2019) 1384–1390.
[23] S. Karan, M.Y. Cho, H. Lee, et al., J. Med. Chem. 64 (2021) 2971–2981.
[24] X. Peng, J. Gao, Y. Yuan, et al., Bioconjug. Chem. 30 (2019) 2828–2843.
[25] T. Meng, W. Ma, M. Fan, W. Tang, X. Duan, Anal. Chem. 94 (2022) 10109–10117.
[26] Y. Ji, Y. Wang, N. Zhang, et al., J. Org. Chem. 84 (2019) 1299–1309.
[27] M. Hou, W. Chen, J. Zhao, et al., Chin. Chem. Lett. 33 (2022) 4101–4106.
[28] K. Cai, X. He, Z. Song, et al., J. Am. Chem. Soc. 137 (2015) 3458–3461.
[29] S. Lv, Y. Wu, K. Cai, et al., J. Am. Chem. Soc. 140 (2018) 1235–1238.
[30] Q. Yu, R.M. England, A. Gunnarsson, et al., Macromolecules 55 (2022) 401–412.
[31] Y. Wu, S. Lv, Y. Li, et al., Biomater. Sci. 8 (2020) 949–959.
[32] X. Shi, M. Hou, X. Ma, et al., Biomacromolecules 20 (2019) 1190–1202.
[33] X. Wan, J.J. Beaudoin, N. Vinod, et al., Biomaterials 192 (2019) 1–14.
[34] F. An, J. Xin, C. Deng, et al., J. Mater. Chem. B 9 (2021) 9308–9315.
[35] Z. Thiel, P. Rivera-Fuentes, Angew. Chem. Int. Ed. 58 (2019) 11474–11478.
[36] S. Wang, W. Tan, W. Lang, et al., Anal. Chem. 94 (2022) 7272–7277.
[37] Y. Zhang, J. Zhang, M. Su, C. Li, Biosens. Bioelectron. 175 (2021) 112866.
[38] N. Boens, B. Verbelen, M.J. Ortiz, L. Jiao, W. Dehaen, Coord. Chem. Rev. 399 (2019) 213024.
[39] Y. Fan, M. Lu, X.A. Yu, et al., Anal. Chem. 91 (2019) 6585–6592.
[40] Y. Ji, C. Jones, Y. Baek, et al., Adv. Drug Deliv. Rev. 167 (2020) 121–134.
[41] R. He, D.D. Tang, N.G. Xu, et al., Chin. Chem. Lett. 35 (2024) 108658.
[42] K. Xu, F. Wang, X. Pan, et al., Chem. Commun. 49 (2013) 2554–2556.
[43] S. Sarkar, H. Lee, H.G. Ryu, et al., ACS Sens. 6 (2021) 148–155.